Electronic Supplementary Material (ESI) for Analyst.

Supplementary Information

Unraveling the complex electrochemistry of serotonin using engineered graphitic sensors

Edoardo Cuniberto, Zhujun Huang, Michael D. Ward, Davood Shahrjerdi

Note S1: Effect of the anodic potential on the graphitic sensor structural properties

Fig. S1a shows the background charging current of the graphitic sensor measured at two different anodic potentials (U_a) of 0.6 V and 1.15 V. The data displays that the variation of U_a did not alter the background current shape and amplitude. Moreover, we also observed that the position of the primary redox peaks is not influenced by the change in U_a, as shown in the cyclic voltammograms (CVs) in Fig. S1b. The separation between the redox peaks (ΔE_p) is directly related to the apparent electron transfer rate. Therefore, the data indicate that the apparent electron transfer kinetics of the primary redox couple remain unchanged. Since both the background charging current and the apparent electron transfer rate depend strongly on the structural properties of the graphitic material, we can assert that the U_a does not influence the structural properties of the graphitic sensor. These observations prove that the evolution of the side reaction peak/shoulder as a function of the anodic voltage is not due to a change in the structural properties of the graphitic sensor.

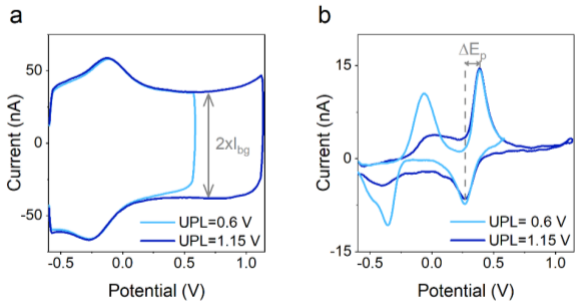

Figure S1: (a) Background charging currents measured at two different anodic voltages of 0.6 V and 1.15 V with cathodic voltage of -0.6 V. (b) Corresponding 5-HT cyclic voltammograms.

Note S2: Effect of sweep rate and cathodic potential on the secondary reaction

Our experiments revealed that the CVs of 5-HT strongly depend on the anodic potential of the FSCV waveform. Further, we hypothesized and established experimentally that the well-defined secondary redox couple observed for U_a<0.8 V arises from the nucleophilic attack of water on the

quinone imine. We also examined experimentally the effect of other FSCV parameters (cathodic potential and sweep rate) on the secondary reactions.

In these experiments, we initially performed 5-HT measurements at faster sweep rates while keeping U_a<0.8 V to avoid water oxidation. Fig. S2a shows the normalized background-subtracted CVs of 500 nM 5-HT measured at ν=200, 400 and 800 V.s^{-1}. The data indicate an expected shift in redox potentials and broadening of the peaks by increasing the sweep rate. Importantly, the data revealed that the secondary redox couple persists at these high sweep rates. Since the CVs look qualitatively the same, we concluded that increasing the sweep rate (up to 800 V.s^{-1}) had negligible effect on mitigating the secondary reaction due to the nucleophilic attack.

Next, we investigated the effect of the cathodic potential (U_c). In the main manuscript, we selected a cathodic potential of -0.6 V to achieve a complete reduction peak for the secondary product. However, most FSCV studies do not sweep to cathodic potentials this low. The typical U_c is -0.4 V. Fig. S2b compares the normalized CVs obtained with U_c=-0.4 and -0.6 V. The data indicate that this choice of the cathodic potentials has no detectable effect on the secondary redox reaction.

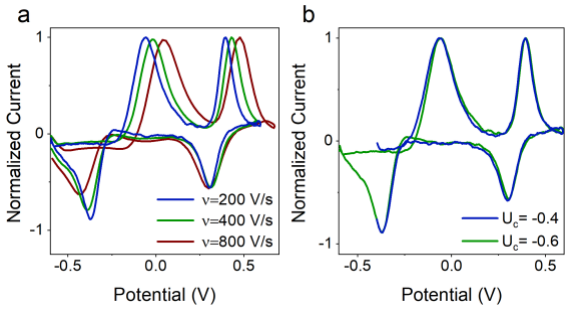

Figure S2: (a) Normalized background-subtracted CVs of 500 nM 5-HT measured at ν=200, 400, and 800V.s^{-1}. (b) Normalized background-subtracted CVs of 500 nM 5-HT measured at U_c=-0.4 and -0.6 V.

Note S3: Generalizability of the anodic potential effect on 5-HT electrochemistry

We examined whether our observations from the engineered graphitic sensors on the effect of U_a can be generalized to carbon fiber micro-electrodes (CFME). Therefore, we performed experiments on commercially available CFME, in which we employed a triangular waveform with a fixed cathodic potential of -0.4 V and only varied the anodic potential. Fig. S3 shows the CVs of 5-HT measured at different U_a values at a sweep rate of 200 V.s^{-1}. This sweep rate allows the comparison of CVs from CFME against those of our graphitic sensors.

The data revealed a noticeable change in the shape of the oxidation peak associated with the side reactions. This oxidation peak evolved from an asymmetric shoulder-like peak at U_a=1.3 V to a more separated and nearly symmetric peak at U_a=0.8 V. Notice that the broad peak of the primary 5-HT oxidation peak prevented further measurements at U_a below +0.8 V. Nevertheless, the observed trend here for CFME is consistent with our observations using the engineered graphitic sensors, indicating the generalizability of this phenomenon.

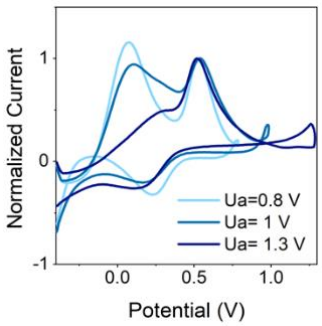

Figure S3: a) Normalized background-subtracted CVs of 500 nM 5-HT measured at ν=200 V.s^{-1} using triangular waveforms with a cathodic potential of -0.4 V and anodic potentials of +0.8, +1.0, and +1.3 V.

Note S4: Dependence of the secondary reaction on the primary redox couple

Fig. S4a shows the CV of 5-HT obtained with FSCV measurement without flow at U_a=0.2V. The data displays no visible peaks indicating that no secondary reactions are detected. This observation reveals the strong dependence of the secondary reaction on the primary redox couple. Specifically, it shows that without the electrooxidation of 5-HT there is no secondary reaction taking place. Fig. S4b displays the CV of 5-HT with a U_a=0.35 V. This potential is not sufficient for a complete redox reaction of 5-HV, however it is enough to trigger the oxidation of the side product. This results further corroborate the necessity of 5-HT oxidation for the initiation of the secondary reaction. Finally, Fig S4c-d shows that more is the 5-HT oxidation complete, higher will be the peak current of the secondary reaction.

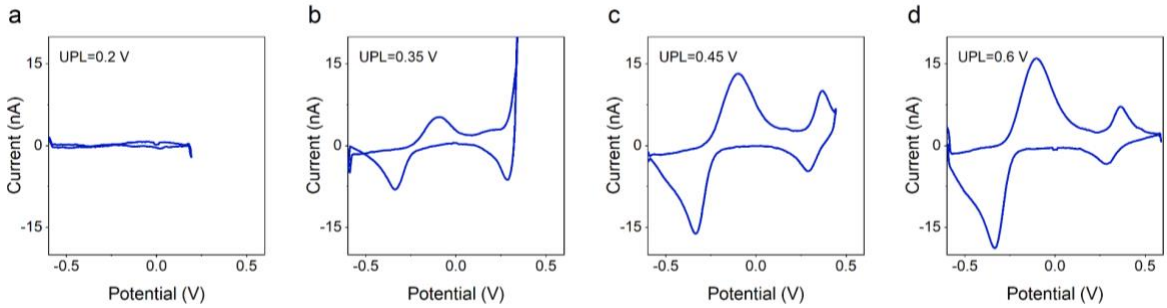

Figure S4: Cyclic voltammograms of 500 nM 5-HT obtained at different anodic potentials of (a) 0.2 V, (b) 0.35, (c) 0.45, and (d) 0.6 V. The data indicate that the secondary redox peaks appear only when the anodic voltage is high enough for oxidation of 5-HT.

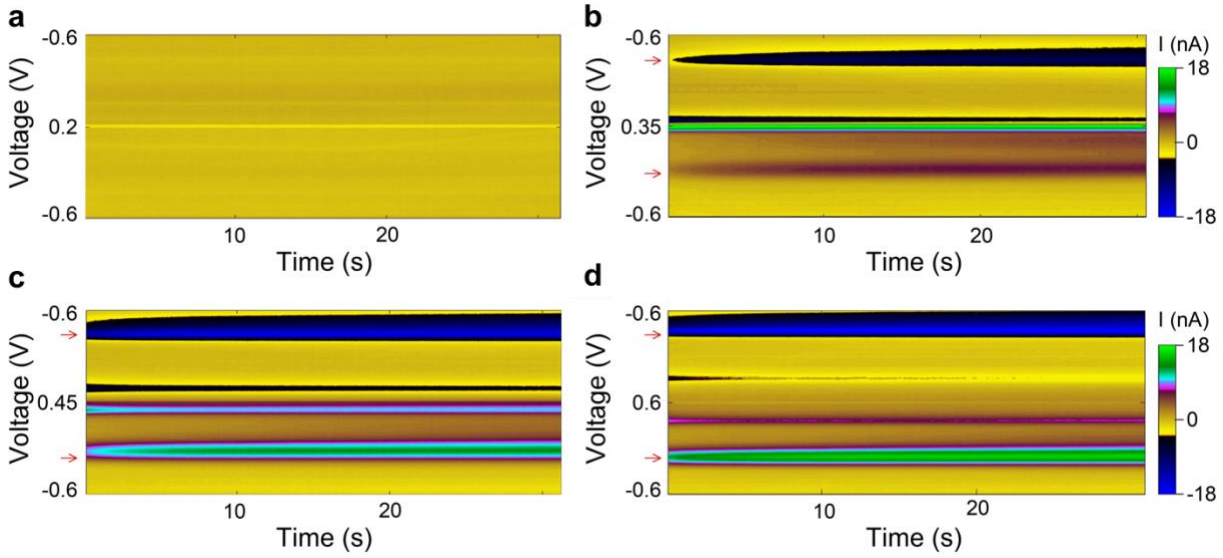

Figure S5: Reproduction of Fig.3 of the main manuscript. The color maps are plotted using the conventional non-linear FSCV color scale.

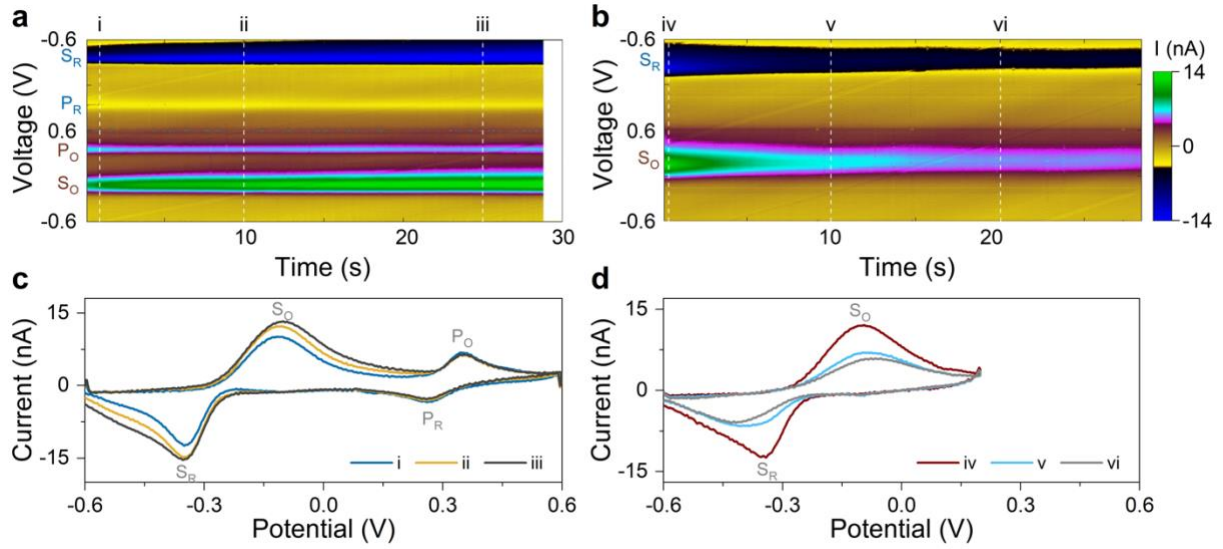

Figure S6: Reproduction of Fig.4 of the main manuscript. The color maps are plotted using the conventional non-linear FSCV color scale.